Solid Freeform Fabrication 2018: Proceedings of the 29th Annual International Solid Freeform Fabrication Symposium – An Additive Manufacturing Conference
Reviewed Paper

Mechanical Properties Evaluation of a Ti-6Al-4V Thin-Wall Structure Produced by a Hybrid Manufacturing Process

Lei Yan[1,4], Wenyuan Cui[1], Joseph W. Newkirk[2], Frank Liou[1], Eric E. Thomas[3], Andrew H. Baker[3], James B. Castle[3]

[1]Department of Mechanical and Aerospace Engineering
[2]Department of Materials Science and Engineering
Missouri University of Science and Technology, Rolla, MO, USA
[3]The Boeing Company, St. Louis, MO
[4]Email: lyvh8@mst.edu, lei.aaron.yan@gmail.com

Abstract

The hybrid manufacturing (HM) process combines the precision of computer numerical control (CNC) and the freeform capability of additive manufacturing to expand the versatility of advanced manufacturing. The intent of this paper is to explore the relationship between HM processing parameters and mechanical properties of the final parts manufactured by one type of HM process that combines laser metal deposition (LMD) and CNC milling. The design of experiment (DOE) is implemented to explore the Ti-6Al-4V thin-wall structure fabrication process with different HM build strategies. Vickers hardness, tensile test, and microstructure analyses are conducted to evaluate the mechanical property variance within the final parts fabricated according to the DOE matrix. Finally, a prediction model of yield strength at 0.2% offset for Ti-6Al-4V parts built through the aforementioned HM process was obtained by an analysis of variance (ANOVA) test, which revealed the significant factors are build height within each LMD process, laser energy input, and the interaction of build height within each LMD process to the preheating condition.

Introduction

Laser metal deposition (LMD) has made many breakthrough successes in complex parts fabrication and new materials development [1-4]. However, due to the inherent rapid solidification rates of the LMD process, conditions that favor porosity, distortion, and rough surface finish of LMD build parts usually requires post-heat treatment and machining to meet end-use dimensional and mechanical requirements [5-7]. Hybrid Manufacturing (HM) offers an opportunity to combine deposition and a suite of in-situ processing techniques such as machining and inspection. The HM process combines the freeform capability of additive manufacturing with the precision of computer numerical control (CNC) to enable done-in-one ability, allows in-process quality inspection, and provides solutions to address inner features machining problems; one such example is the machining of channels in an engine manifold. In recent years, many efforts have been put forth on the development of different types of HM systems. One example is the integration of a laser welding system, five-axis milling center, and a custom PCNC-based control unit successfully produced injection molding dies [8]. A hybrid rapid prototyping process which combines a six-axis machining center with potentially any kind of additive manufacturing deposition process and accordingly, an advanced process planning system, has also been investigated. The planning

system partitions the part into 3D manufacturable volumes from its CAD model and provides a feasible process plan for the whole building process [9]. To produce near-net shape tools and dies, in-process face milling operations were introduced to a direct rapid tooling system, where a TransPulse Synergic MIG/MAG welding process was integrated with a conventional face milling process to control the desired layer height after each welding operation [10]. A comparable manufacturing solution integrated a laser system into a conventional milling machine where the manufacturing accuracy was controlled by milling the surface after each deposition [11]. The ability of the HM process was expanded by utilizing two welding guns or filling deposited shells to deposits with two materials simultaneously [12]. The introduction of a new integrated production system which performs laser cladding, machining, and in-process inspection in a single machine for turbine blade repair provided new ideas for improving the flexibility and lean manufacturing in the advanced manufacturing industry [13]. Today, some commercial HM machines have been introduced to the market such as Mazak Corporation's INTEGREX i-400 AM machine and DMG Mori's Lasertec hybrid machines. Those machines utilize narrow beam diameter high-speed laser metal deposition heads, machining, and contact inspection to increase both the production rate and part accuracy. Until now, research on the HM process has mainly focused on machine hardware and motion control package development; minimum effort has been placed on investigating how mechanical properties and microstructure evolution in the final part is related to the HM processing parameters. In this paper, experiments of fabricating Ti-6Al-4V thin-wall structures are conducted to understand how different HM build strategies are linked to the variance of Vickers hardness, yield strength and microstructural features of material produced by the HM process. The thin-wall structures were fabricated according to a design of experiments (DOE) matrix where layer height, laser energy input, powder feed rate, and preheat conditions were selected as input factors. The significant factors impacting yield strength (YS) are obtained based on the analysis of variance (ANOVA) test of the tensile test results and an empirical linear regression YS prediction model is provided.

Materials and Methods

Here, the additive and subtractive processes were conducted in two separate systems, LMD and CNC milling, but with the same processing procedures as would be conducted in an integrated HM system. Theoretically, the conclusions drawn from current research will benefit experiment design and process optimization on an integrated hybrid machine. Though this research is focused on small-scale part fabrication, the results can be used to investigate and provide guidelines for large-scale part fabrication.

Sample fabrication

Thin-wall samples were fabricated using an in-house laser metal deposition (LMD) system, as shown in Fig. 1 (a). The laser system is a 1 kW Nd-YAG fiber laser (IPG Photonics, MA, USA) and deposition with a 2 mm beam diameter. The working principle of the implemented powder delivery system (Powder Motion Labs, MO, USA) is mainly based on powder gravity and guarantees a small powder stream divergence angle. Powders used in this research are gas atomized Ti-6Al-4V powders (Advanced Specialty Metals, NH, USA) with size -60+120 mesh. Grade 5 Ti-6Al-4V plates (ATI, PA, USA) with dimensions 75 mm x 25 mm x 7 mm were used

as the substrate. Thin-wall deposits were fabricated in an argon purged chamber, where the substrates were clamped on a three-axis numerical control work table, and the motion control was coded in LinuxCNC.

For machining in between the additive processes, the subtractive processes were conducted on a PCNC 1100 CNC mill (Tormach, WI, USA) with a 0.5'' Iscar insert cutter (Iscar, Migdal Tefen, Israel). The LMD-fabricated Ti-6Al-4V part does not behave like a Ti-6Al-4V billet and modification to standard machining recipes were required. Final cutting parameters were set to 450 sfm and .0027 chip per tooth, with Hocut 795 B cutting fluid (Houghton, PA, USA), which produced good cuts with the quality surface finish and longer insert life. Keeping the deposit well aligned during transitions between multiple depositions and machining procedures in the HM process is critical to maintaining the final product's geometry. This accuracy requirement necessitated designing two sets of fixtures to solve this issue. The fixture used in the deposition process is shown in Fig. 1 (b); three pins and a toggle clamp were used to guarantee the alignment during each transition. Fig. 1 (c) shows the fixture used in machining, which has a similar design using pins and nuts for aligning and fixing purposes.

HM build strategies

The illustration of the HM process is demonstrated in Fig. 1 (e). Milling was conducted on each deposition's top surface to achieve the designed height and prepare for the next deposition. A certain height of the non-machined as-deposit side surfaces, designated as shielding height, is left to protect the machined surfaces from being spoiled by the following deposition process. The deposit height in between each machining process is called layer height. The material thickness was removed at each side is referred to as depth of cutting.

(a) (b) (c)

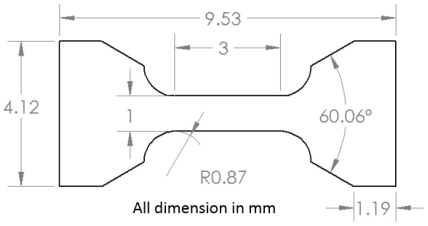

(d)

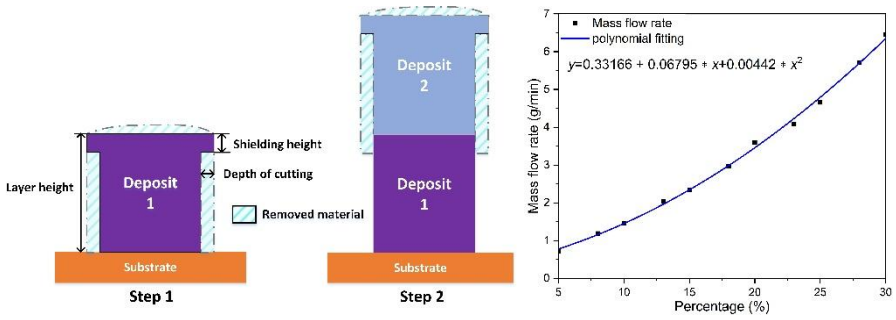

(e) (f)

Fig. 1 Experimental set-up. (a) LMD process schematic, (b) fixture for LMD process, (c) fixture for milling process, (d) tensile test sample, (e) HM schematic, (f) powder feed rate calibration results.

Laser energy input is a critical factor that directly relates to overheating or lack of fusion in the deposition process. Only considering laser power or laser transverse speed is inappropriate for deposition process control because the combination of laser power and laser transverse speed actually matters [16]. To implement the combination effect of laser power and laser transverse speed, the concept of laser energy density (LED) is proposed and defined as $LED = p/v$, where p is laser power (in Watts) and v is laser transverse speed (in mm/min). Based on the preliminary study of the deposition quality on the three-axis numerical control work table, laser transverse speed was set to 216 mm/min as constant and laser power was modified to explore a suitable LED range. To minimize trial and error, an initial assumption of the minimum energy input needed to melt the introduced powders into the melt pool from the nozzle was conducted based on $Q = m * \Delta T * C_p$ and the latent heat of fusion L, where m denotes the mass of the melted powders, ΔT is set as the powder temperature change from ambient temperature 300 K to the melting point 1933 K, and C_p is specific heat capacity. The energy efficiency of the LMD process with YAG laser is shown to be only 10-20% of the raw power to be used for powder melting purposes [17]. The thickness of the machined thin-wall structure was designed to 2 mm and required the rough thickness before milling to be around 3 to 3.5 mm. A suitable single track height that yields a stable build-up with good powder capture efficiency was 0.5 mm. Using a laser transverse speed of 216 mm/min, a single track height 0.5 mm, a wall thickness of 3.5 mm, and the latent heat of fusion of 370 kJ/kg for calculation, the minimum LED needed to melt all the introduced powder is 1.38 W/(mm/min) and the relative laser power is 298 W. A suitable range was determined for a fully dense part fabrication and the avoidance of severe overheating from 1.6 to 1.7 W/(mm/min) and corresponds to laser power 345 W and 367 W, respectively. For powder mass flow rate control with the selected Ti-6Al-4V powders, calibration work on the powder feeder was conducted and the result is as shown in Fig. 1 (f), where the x-axis denotes the percentage of the full feeding speed at testing and the y-axis denotes the actual powder weight gathered at each selected feeding speed within a minute. The feeding speed from 5% to 30% was tested; less than 5% leads to lack of powder to build the thin-wall with required thickness, and more than 30% results in a waste of powders and causes powder to sinter on the deposit side surfaces. The experimental data was polynomial fitted with adjusted r-square value of 0.99696. To make thin-wall structures with a

thickness around 3 to 3.5 mm and avoid severe issues of powder sintering on surfaces, the powder feeder mass flow rate was determined to be between 1.45 g/min and 1.96 g/min. Scanning electron microscopy (SEM) images of the deposit's cross sections revealed a full dense part and no fusion defects, indicating sufficient LED input.

A design of experiments (DOE) approach was implemented to explore the impacts of different build strategies on mechanical properties and microstructure evaluation of the final parts. Four processing parameters: layer height, powder feed rate, laser energy density (LED), and preheating conditions were selected as input variables for a screening DOE. Considering the accuracy and time efficiency, a four-factor two-level half-fractional DOE matrix was designed, consisting of $2^{4-1} = 8$ runs (resolution IV design). For layer height, 4 mm and 6 mm were selected as the low- and high-level value, respectively. These two height values were easily obtainable and had enough height difference for small-scale model analysis with the DOE matrix. The total height of the final part was set to 12 mm, which meant the final part for the 4 mm layer scenario required performing the deposition and machining procedures three times each, and the 6 mm layer scenario required performing each procedure twice. To reduce residual stress magnitudes and warping, preheating the solid mass before subsequent deposition was considered [18]. The preheating requirement was fulfilled by laser scanning along the predefined deposition path. The four-factor, two-level, one-half fractional design was generated with suitable low level and high level for the selected parameters as shown in Table I and the corresponding DOE matrix is in Table II, a resolution IV design with eight runs total.

Table I: Parameter Set-up in the DOE

Label	Parameters	Low level (-)	High level (+)
A	Layer height	4 mm	6 mm
B	Powder feed rate	1.45 g/min	1.96 g/min
C	Energy density	1.6 W(mm/min)	1.7 W/(mm/min)
D	Preheat	No preheat	Preheat

Table II: DOE Matrix

A design with the Defining Relation I=ABCD

	basic design				
Run	A	B	C	D=ABC	Treatment combination
1	-	-	-	-	(1)
2	+	-	-	+	ad
3	+	+	-	-	ab
4	-	+	-	+	bd
5	+	-	+	-	ac
6	-	-	+	+	cd
7	-	+	+	-	bc
8	+	+	+	+	abcd

Mechanical properties and microstructure analyses

To evaluate mechanical performance, Vickers hardness and tensile tests were conducted. Vickers hardness tests were used to analyze how different HM build strategies affect the hardness distribution along deposit build height direction. Cross sections of the final thin-wall structures

were cut by electrical discharge machining (EDM) on a Hansvedt DS-2 (Hansvedt, IL, USA), mounted on a Buehler SimpliMet 1000 (Buehler, IL, USA) with Bakelite resin (Leco, MI, USA), and polished on a Leco SS 1000 (Leco, MI, USA) according to a standard Ti-6Al-4V metallographic procedure [15]. Kroll's reagent was prepared by mixing 92 ml distilled H_2O, 6 ml HNO_3 (Fisher Chemical, MA, USA), and 2 ml HF (Fisher Chemical, MA, USA) and applied as an etchant to accentuate phase differentiation. The etched samples were then tested with a 0.05 kgf load and 30 s dwell time on the Leco hardness tester V-100-42 (Leco, MI, USA). Vickers hardness sampling points were distributed along three zigzag routes at 0.3 mm intervals, and the Vickers hardness at certain heights was taken from the average Vickers hardness number of each row with the same height.

Tensile tests were conducted to evaluate the yield strength for HM thin-wall structures. Test samples were prepared with EDM cuts according to the dimensions in Fig. 1 (d) with 1 mm thickness. For each 12 mm height sample prepared with 6 mm layer height, tensile test samples were prepared with bonding areas at a 6 mm height within the gauge length. For 4 mm layer height cases, there are two bonding areas at 4 mm and 8 mm heights. Different tensile test samples were cut to have those two bonding areas covered within the gauge length and the one with a lower yield strength (YS) at 0.2% offset value was considered as a response for the ANOVA test. All the EDM cut samples were polished with 800 grit sandpaper (Leco, MI, USA) to remove microcracks within the gauge length before testing. Tensile tests were conducted on an Instron 5966 machine (Instron, MA, USA) at test speed 0.015 mm/mm/min.

Results and Discussion

Mechanical properties and microstructure analyses

Eight thin-wall structure samples were fabricated according to the DOE matrix as shown in Fig. 2 (a), where the final dimensions of each thin-wall sample is 18 mm x 2 mm x 12 mm.

Vickers hardness tests were performed according to the procedures discussed in the sample fabrication section and the results are plotted in Fig. 2 (b) and Fig. 2 (c), where Fig. 2 (b) represents the hardness distribution along build height direction within samples fabricated with a 4 mm layer height and Fig. 2 (c) shows results of samples fabricated with a 6 mm layer height. Those two figures depict that all the deposits are harder than Ti-6Al-4V Grade 5 plate. The Vickers hardness value is relatively lower at the heat affect zone on the substrate compared to deposits because of the formation of nearly lamellar structures caused by the lower cooling rate there in the deposition process [19]. The hardness distribution is different for each sample, but follows a similar trend compared to the two samples deposited with the non-stop process. At each stop position in both the 4 mm and 6 mm layer height scenarios, no sudden hardness changes were observed. The average Vickers hardness values were evaluated and labeled on the top right in Fig. 2 (b) and Fig. 2 (c). Vickers hardness comparisons between different layer height scenarios shows the 6 mm ones tend to have a slightly higher hardness value than the 4 mm, which comes from more low-temperature thermal mass, the previously deposited and machined thin-wall structure beneath current fabricating layers. Reducing heat during the deposition process will lead to a higher cooling

rate and result in fine microstructure formations, and accordingly, leads to a higher Vickers hardness result.

The average YS of Ti-6Al-4V samples prepared with the laser deposition system is 925 MPa [20]. The average YS at 0.2% offset of the thin-wall structures fabricated non-stop on preheated substrates is 994.7 MPa. An average value of 993.9 MPa was obtained on room temperature substrates. The tensile test results of the samples made through the DOE matrix are listed in Table III. Samples fabricated under the set-up of the first run from the DOE matrix have a lower YS value compared to the other seven runs. This particular run was fabricated with a 4 mm layer height and had two bonding areas within the deposit, where the YS of 834.0 MPa and 965.9 MPa were obtained and the lower value 834.0 MPa was selected to represent the YS of the thin-wall sample.

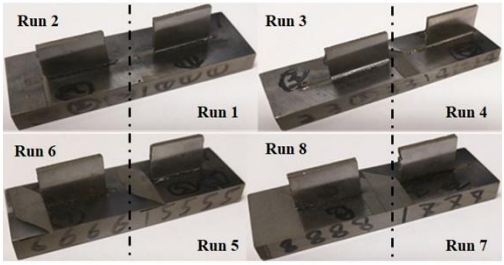

(a)

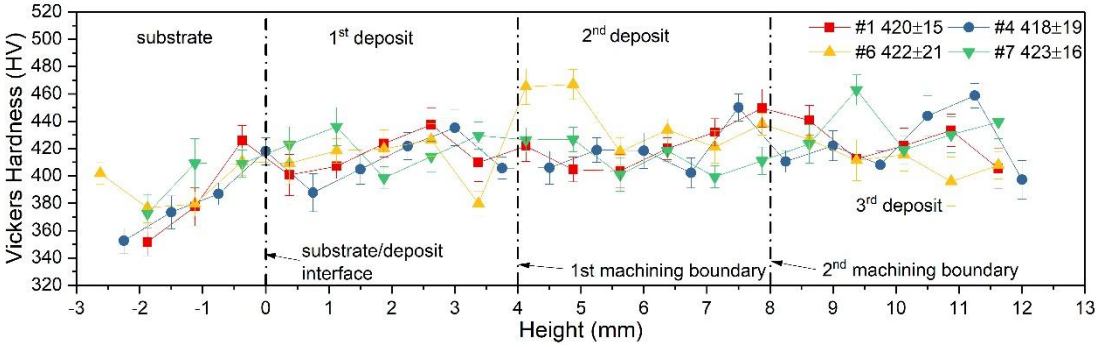

(b)

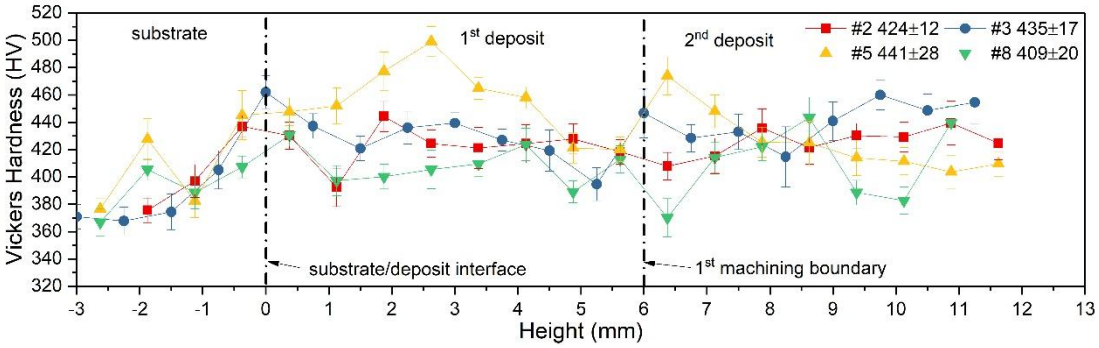

(c)

Fig. 2 Final structures and Vickers hardness results. (a) machined final product, (b) Vickers hardness results at layer height 4 mm scenario, (c) Vickers hardness results at layer height 6 mm scenario.

Table III: YS & UTS data

Run No.	YS (avg.) at 0.2% offset (MPa)	UTS (avg.) (MPa)
1	834	959
2	961	1036
3	1022	1074
4	1004	1086
5	1049	1104
6	1001	1044
7	932	1044
8	925	1000

To better understand the Vickers hardness and tensile tests results, microstructure characterization was conducted on a digital microscope (Hirox, NJ, USA) from the substrate to the top of the deposits. The characterization results showed grain boundary alpha, martensitic-alpha, and primary-alpha (colony and basketweave) morphologies, with a basketweave morphology being was the predominant type as shown in Fig. 3, which tends to form with an increased cooling rate from the β-phase field and is consistent with previous findings [21-22]. A general trend was the microstructure would be finer when closer to the bottom due to a larger cooling rate at the beginning of the deposition [23].

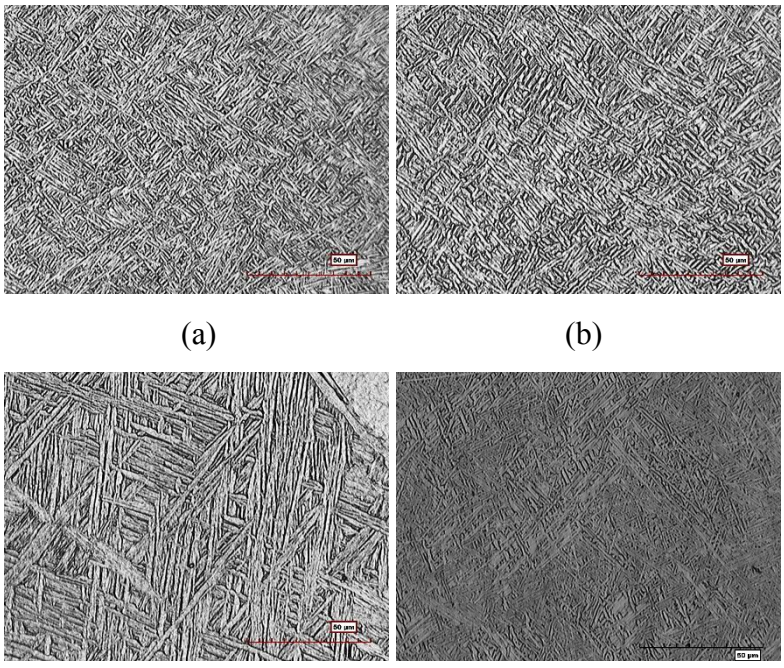

(a) (b)

(c) (d)

Fig. 3 Typical microstructure in the final deposits. (a) at the bottom of the deposit, (b) at the middle of the deposit, (c) at the top of the deposit, (d) at the substrate and deposit boundary (run 8).

ANOVA test

The ANOVA test was conducted in SAS™ based on the YS data acquired from the tensile tests. The test was conducted according to the standard analyze procedures of a four-factor, two-level, half-fractional design [24]. To demonstrate the significance of tested factors, the YS data was analyzed by constructing a normal probability plot of the effects for each factor as shown in Fig.4 (a), where all of the effects along the line are negligible, and greater effects are farther from the line. [25]. The ANOVA test result shows that layer height, energy density, and the interaction of layer height and preheating condition has significant impacts on the YS of the Ti-6Al-4V parts. The predicted YS model is described with significant factors and written as:

$$YS = 965.9 + 23.39X_1 + 10.71X_3 - 52.96X_1 * X_4,$$

where 965.9 is the average response. X_1, X_3, and X_4 take on values between -1 and 1, which denote three selected factors: layer height, energy density, and preheat condition, respectively.

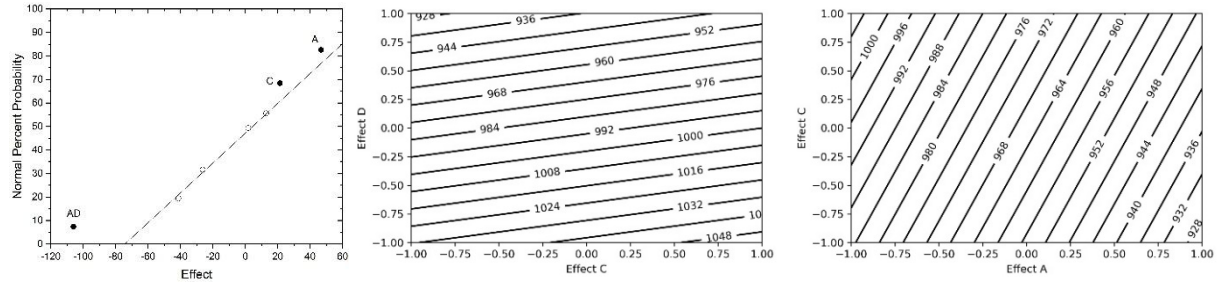

a b c

Fig. 4 DOE analyses results. (a) effects normal probability, (b) contour plot with$X_1 = 1$, (c) contour plot with $X_4 = 1$.

The response surface is generated by the YS regression model and is shown in Fig. 4. Fig. 4 (b) shows the response surface contour plot when X_1 is at a high level and takes on value 1, which indicates no preheat and high energy density tends to increase the YS of the final part. Fig. 4 (c) shows the response surface contour plot when X_4 is at a high level and takes on value 1, which indicates high energy density and low layer height tends to benefit the increase of YS. The contours have curved lines which means the model contains an interaction term. The contour plot provides a detailed insight to the YS evolution with the changes of different processing parameters.

Conclusions

In conclusion, we investigated the fabrication process of Ti-6Al-4V thin-wall structures with different hybrid manufacturing strategies. The evaluation of Vickers hardness and characterization of microstructures showed that similar hardness distribution and microstructures can be obtained compared to the non-stop deposition process. The ANOVA test results provide a better understanding of the relationship between processing parameters and YS (at 0.2% offset).

Furthermore, the conclusions drawn from this study will benefit small features fabrication and provide guidelines for large-scale part manufacturing with the hybrid manufacturing process.

Acknowledgments

This project was supported by The Boeing Company through the Center for Aerospace Manufacturing Technologies (CAMT), National Science Foundation Grants #CMMI-1547042 and CMMI-1625736, and the Intelligent Systems Center (ISC) at Missouri S&T. Their financial support is greatly appreciated.

References

[1] W. Li, L. Yan, S. Karnati, F. Liou, J. Newkirk, K. M. B. Taminger, W. J. Seufzer, Ti-fe intermetallics analysis and control in joining titanium alloy and stainless steel by laser metal deposition, Journal of Materials Processing Technology 242 (2017) 39-48.

[2] Chen, Danfang, et al. "Direct digital manufacturing: definition, evolution, and sustainability implications." Journal of Cleaner Production 107 (2015): 615-625.

[3] Laeng, James, J. G. Stewart, and Frank W. Liou. "Laser metal forming processes for rapid prototyping-A review." International Journal of Production Research 38.16 (2000): 3973-3996.

[4] L. D. Bobbio, R. A. Otis, J. P. Borgonia, R. P. Dillon, A. A. Shapiro, Z.-K. Liu, A. M. Beese, Additive manufacturing of a functionally graded material from ti-6al-4v to invar: Experimental characterization and thermodynamic calculations, Acta Materialia (2017).

[5] D. Homar, F. Pusavec, The development of a recognition geometry algorithm for hybrid-subtractive and additive manufacturing, Strojniski vestnik-Journal of Mechanical Engineering 63 (2017) 151-160.

[6] T. Yamazaki, Development of a hybrid multi-tasking machine tool: Integration of additive manufacturing technology with cnc machining, Procedia CIRP 42 (2016) 81-86.

[7] Z.-p. Ye, Z.-j. Zhang, X. Jin, M.-Z. Xiao, J.-z. Su, Study of hybrid additive manufacturing based on pulse laser wire depositing and milling, The International Journal of Advanced Manufacturing Technology (2016) 1¬12.

[8] Choi, Doo-Sun, et al. "Development of a direct metal freeform fabrication technique using CO2 laser welding and milling technology." Journal of Materials Processing Technology 113.1-3 (2001): 273-279.

[9] Hur, Junghoon, Kunwoo Lee, and Jongwon Kim. "Hybrid rapid prototyping system using machining and deposition." Computer-Aided Design 34.10 (2002): 741-754.

[10] Akula, Sreenathbabu, and K. P. Karunakaran. "Hybrid adaptive layer manufacturing: An Intelligent art of direct metal rapid tooling process." Robotics and Computer-Integrated Manufacturing 22.2 (2006): 113-123.

[11] Klocke, F. "Rapid Manufacture of Metal Components." Fraunhofer Institute for Production Technology, IPT, Aachen, Germany (2002).

[12] Song, Yong-Ak, and Sehyung Park. "Experimental investigations into rapid prototyping of composites by novel hybrid deposition process." Journal of Materials Processing Technology 171.1 (2006): 35-40.

[13] Jones, Jason B., et al. "Remanufacture of turbine blades by laser cladding, machining and in-process scanning in a single machine." (2012).

[14] Yamazaki, Taku. "Development of a hybrid multi-tasking machine tool: integration of additive manufacturing technology with CNC machining." Procedia CIRP 42 (2016): 81-86.

[15] L. Yan, X. Chen, W. Li, J. Newkirk, F. Liou, Direct laser deposition of ti-6al-4v from elemental powder blends, Rapid Prototyping Journal 22 (2016) 810-816.

[16] Santhanakrishnan, Soundarapandian, Fanrong Kong, and Radovan Kovacevic. "An experimentally based thermo-kinetic hardening model for high power direct diode laser cladding." Journal of Materials Processing Technology 211.7 (2011): 1247-1259.

[17] Salonitis, Konstantinos, et al. "Additive manufacturing and post-processing simulation: laser cladding followed by high speed machining." The International Journal of Advanced Manufacturing Technology 85.9-12 (2016): 2401-2411.

[18] A. Vasinonta, J. Beuth, M. Griffith, Process maps for laser deposition of thin-walled structures, in: Solid Freeform Fabrication Proceedings, The University of Texas at Austin, August, pp. 383-391.

[19] Maliutina, Iuliia Nikolaevna, Hocine Si-Mohand, Romain Piolet, Florent Missemer, Albert Igorevich Popelyukh, Natalya Sergeevna Belousova, and Philippe Bertrand. "Laser cladding of γ-TiAl intermetallic alloy on titanium alloy substrates." Metallurgical and Materials Transactions A 47, no. 1 (2016): 378-387.

[20] Dey, Nanda Kumar. Additive manufacturing laser deposition of Ti-6Al-4V for aerospace repair application. Missouri University of Science and Technology, 2014.

[21] Kelly, S. M., and S. L. Kampe. "Microstructural evolution in laser-deposited multilayer Ti-6Al-4V builds: Part I. Microstructural characterization." Metallurgical and Materials Transactions A 35.6 (2004): 1861-1867.

[22] Fu, Tian, et al. "Microstructural characterization of diode laser deposited Ti-6Al-4V." Missouri University of Science and Technology, Proceedings of the 19 th Annual SFF Symposium, Austin, Tx., pp110-115. 2008.

[23] Yan, Lei, et al. "Direct laser deposition of Ti-6Al-4V from elemental powder blends." Rapid Prototyping Journal 22.5 (2016): 810-816.

[24] Montgomery, Douglas C. Design and analysis of experiments. John wiley & sons, 2017.

[25] Yan, Lei, Yunlu Zhang, and Frank Liou. "A conceptual design of residual stress reduction with multiple shape laser beams in direct laser deposition." Finite Elements in Analysis and Design 144 (2018): 30-37.